PHYSICAL REVIEW C VOLUME 45, NUMBER 3 MARCH 1992

ARTICLES

Absolute measurement of the differential cross section for deuteron photodisintegration from 63 to 71 MeV

P. T. Debevec, P. D. Harty,* and J. E. Knott†
Nuclear Physics Laboratory and Deptartment of Physics, University of Illinois at Urbana-Champaign, Champaign, Illinois 61820

D. A. Jenkins and R. T. Jones‡
Physics Department, Virginia Polytechnic Institute and State University, Blacksburg, Virginia 24061
(Received 9 December 1991)

The absolute differential cross section for the $^2\mathrm{H}(\gamma,p)n$ reaction has been measured using a large solid angle detector, with a tagged photon beam of mean energy 67 MeV. The data have been compared with nine different theoretical calculations of the cross section, which account for the data to varying degrees. Best agreement is obtained for models utilizing the nonrelativistic impulse approximation with a realistic nuclear potential, meson-exchange currents and relativistic corrections.

PACS numbers: 25.10.+s, 25.20.−x

I. INTRODUCTION

The relative simplicity of the deuteron and the low perturbative effect of the photon probe make the deuteron photodisintegration reaction very attractive for the testing of various theoretical descriptions. These include models of the NN interaction, meson-exchange currents (MEC), isobar configurations (IC), relativistic corrections (RC), and quark-gluon degrees of freedom. Recently Arenhövel and Sanzone have written a thorough review of deuteron photodisintegration and have made extensive comparisons between the latest theories and data [1]. They find that, although several theories are able at present to account for the experimental data, more extensive and precise data sets are needed to confront these theories.

Previous data on the $^2\mathrm{H}(\gamma,p)n$ reaction, in the energy region around 65 MeV, are sparse, and some of the data have large systematic errors in the absolute scale [2–9]. Some of the early measurements have had problems with the absolute normalization, due to the use of bremsstrahlung beams. These early measurements generally suffered from inaccurate determinations of the photon flux and energy. In this energy range the capture reaction, $^1\mathrm{H}(n,\gamma)^2H$, has also been measured [10, 11]. Most of these measurements are not precise enough to differentiate among the various theoretical calculations of the cross section.

The present measurement, in the energy range $E_\gamma = 63$ to 71 MeV and covering angles from 22.5° to 160.5° with statistical errors of about 5%, can differentiate between various theoretical models. The tagged photon beam allows an accurate determination of the absolute scale of the cross section, which has an error of about 4%, over most of the angular range. The use of a detector with large solid angle (LASA detector), allows the measurement to extend over a wide range of angles, providing a stringent test of the angular distribution behavior of the theoretical curves.

II. THEORY

Nine different theoretical calculations of the differential cross section will be considered for comparison with the data. These theories represent a broad spectrum of efforts that have endeavored to incorporate the complexities of the structure of the deuteron, the neutron-proton interaction, and the electromagnetic current into a complete and self-consistent calculation. Several of these calculations have been refined over the past decade and have reached an impressive level of sophistication. There are actually many similarities among these calculations, although the differences among them are more often noted.

The first of these calculations is by Partovi [12]. His calculation, which makes a multipole decomposition of the transition amplitude, was the first to include electric and magnetic multipoles through dipole-octupole interference. The semiphenomenological Hamada-Johnston [13] potential was used in computing wave functions. The dominant part of the MEC is included implicitly by

---

*Present address: Kelvin Laboratory, University of Glasgow, Glasgow G12 8QQ, Scotland.

†Present address: Indiana University Cyclotron Facility, 2401 Milo B. Sampson Lane, Bloomington, IN 47405.

‡Present address: CERN, CH-1211 Geneva 23, Switzerland.

the use of the Siegert operators for electric transitions. However, no explicit MEC beyond these are included. This calculation suffers also from the lack of important RC such as the spin-orbit contribution to the one-body charge density.

Three of the calculations are very similar to each other, those by Schmitt and Arenhövel (SA) [14], Cambi, Mosconi, and Ricci (CMR) [15], and Jaus and Woolcock (JW) [16]. They all start with the nonrelativistic impulse approximation (IA) using realistic potentials, the Bonn r-space potential in the case of SA, and the Paris potential for CMR and JW. All multipoles through $L = 4$ are included. MEC are included implicitly by use of the Siegert operators with additional MEC beyond these included explicitly. These calculations have similar, but by no means identical, formulations of the MEC. RC are made by all three calculations for the spin-orbit current and further relativistic contributions. The calculations all differ in their calculation of the IC contribution [1], but the effect is small at the energies of the present measurement.

Also, the calculation by Rustgi, Pandey, and Kassaee (RPK) will be compared to the data [17]. Unlike the above calculations, RPK formulate the problem in terms of spin-angle functions, which are closely related to the twelve invariant amplitudes. The Paris potential is used to calculate the wave functions. Only $E1$, $M1$, and $E2$ amplitudes are used for the present results, although higher multipoles could have been included. Explicit MEC are included, and RC are made to the one-body and two-body charge and current densities, with their local and nonlocal contributions.

Another of the calculations to be compared with the data is by Ying, Henley, and Miller (YHM) [18]. They start with the nonrelativistic IA using the Bonn potential, similar to the calculation by SA, and include MEC via the Siegert operators. They also calculate contributions from IC and RC in a manner similar to the calculations of SA, JW, and CMR. However, in the calculation of the MEC beyond the Siegert operators, they use the long-wavelength approximation, which appears to slightly underestimate its contribution in the energy region considered here, but significantly underestimates its contribution when the photon energy is larger than 140 MeV [19].

The calculation by Laget [20] uses the diagrammatic approach, where a limited set of diagrams are considered for a given process. In the present calculation Laget includes the nucleon-pole diagrams and the nucleon-pole diagrams with subsequent NN rescattering. This set of diagrams is simply the standard IA formulated in momentum space. The Paris potential is used to obtain the momentum space wave functions. Since the calculation is done in momentum space, no multipole decomposition is performed for the electromagnetic operator (all multipoles are included), and hence no Siegert operators are used. Thus the MEC and IC contributions must be calculated explicitly by including MEC and IC diagrams. In the present calculation, however, MEC and IC diagrams with subsequent NN rescattering are not included. RC are included in all of the diagrams.

The calculation of Govaerts, Lucio, Martinez, and Pestieau (GLMP) uses the low-energy theorem and the effective range approximation to calculate a relatively simple formula for the unpolarized photodisintegration cross section [21]. The dominant component of the angular distribution is basically $\sin^2\theta$ electric dipole, with a relativistic correction factor of $(1 - v\cos\theta)^{-2}$, where v is the center-of-mass (c.m.) nucleon velocity. They suggest that the formula should be applicable at energies up to 80 MeV.

Another calculation that will be compared to the data is the covariant approach of Nagornyi, Kasatkin, Inopin, and Kirichenko (NKIK) [22]. They use a field-theoretical method to treat the deuteron, using light front dynamics to determine the wave function from the Paris potential. The calculation endeavors to maintain both gauge and Lorentz invariance. The motivation for this method is the claim that calculations which introduce MEC do so inconsistently and create arbitrarily large uncertainties by significant violations of gauge invariance. However, this criticism has subsequently been addressed by Schmitt *et al.* [19], who find that, if the calculation is done in a gauge with a sensible long-wavelength behavior, the effect of an incompletely conserved current is small numerically.

III. EXPERIMENT

The ^{2}H$(\gamma, p)n$ experiment was performed at the University of Illinois MUSL-2 Accelerator [23], using a tagged photon beam of energy 63 to 71 MeV, in 32 separate channels. Details of the experiment can be found in a separate report [24]. The LASA detector, shown in Fig. 1, and associated electronics have been described in a previous publication [25]. It consists of a cylindrical multiwire proportional chamber for particle tracking, with a cylindrical hole on the central axis where a long tube containing the target gas is placed. Surrounding the chamber there is a scintillator annulus for particle identification and event triggering.

The wire chamber consists of three concentric levels of wires which run parallel to the detector axis. The gas mixture used in the wire chamber for this measurement consisted of 90% argon and 10% methane. In our experiment on helium photodisintegration [26], in order to detect tritons and low-energy protons from many-body breakup, it was necessary to minimize the energy loss of charged particles in the chamber. In that experiment the gas mixture was 90% helium and 10% methane. In

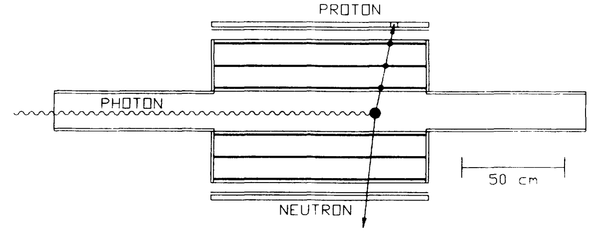

FIG. 1. A schematic diagram of LASA, the large solid angle detector.

deuteron photodisintegration at the photon energies of this experiment, the energy loss of the protons in the chamber is not a significant concern.

The scintillator annulus surrounding the wire chamber consists of 8 ΔE-E plastic scintillator pairs. The ΔE of each pair is 3.2 mm thick and the E is 25.4 mm thick. An approximately position-independent trigger [25] was derived from an OR of 8 ΔE scintillators and was set in hardware to 1.8 MeV equivalent electron energy (MeVee). This threshold was chosen to be much lower than the average light output of the protons, and therefore allowed flexibility in the later choice of a software threshold, which was effectively 5 MeVee, as discussed below.

The photons were tagged by electrons scattered from a thin bremsstrahlung target. The total number of electrons detected in the $^2\mathrm{H}(\gamma,p)n$ experiment was 4.3 $\times 10^{11}$, distributed fairly evenly over 32 focal plane channels, which tagged photons between 63 and 71 MeV. The position and quality of the electron beam leading to the photon tagger was monitored approximately every hour, in order to assure a stable beam and constant tagging efficiency. The total rate in the focal plane during the photodisintegration measurement was 3×10^6 s^{-1}. The photon tagging efficiency was determined in separate runs, at regular times during the experiment, using a large NaI(Tl) detector placed directly behind the LASA detector. For these tagging efficiency runs, the beam current was four orders of magnitude less intense, so as to prevent damage to the NaI and to minimize random coincidences. In a tagging efficiency run, coincidences between each focal plane counter and the NaI, and singles for each focal plane counter, were recorded. The tagging efficiency, which is the ratio of the number of coincidences to the number of singles, was found to give an average value of 54% per focal plane counter, reproducible to 1%. The number of photons incident at each energy was obtained from the product of the electron counts in each focal plane counter and the average tagging efficiency determined for that counter. The NaI has been calculated to be 0.14% inefficient for photons in the energy range used in this experiment. Due to photon attenuation in the target gas, the 63-μm-thick Mylar target window, and the air in front of the NaI, there was a further 0.27% loss of photons before the NaI, as compared to the target center. Correction has been made for this combined loss of 0.41%.

The target bag contained deuterium gas, enriched to the 99.74% level. Impurities in the target were determined by on-line measurement of the gas composition with a chromatograph, and by off-line analysis of the data for two-track events, which cannot be produced by deuteron photodisintegration. The impurities were (0.13 $\pm$ 0.01)% helium and (1.7 $\pm$ 0.4)% air. Since the target could not be evacuated, it was first filled with helium and then flushed with several target volumes of deuterium. A small amount of helium was not removed in this process. The air was found to have entered the bag through a small leak in a seam. The target gas was at room temperature and pressure, which averaged 22.5 °C and 744.1 mm Hg during the experiment. The resultant number density for ^{2}H was 4.86×10^{19} nuclei/cm^3.

IV. ANALYSIS

Since only one charged particle is emitted in the $^2\mathrm{H}(\gamma,p)n$ reaction, the analysis was performed in a single-track mode, essentially as described in detail in a previous publication [26]. In that publication, the geometric acceptance for single-track detection is described, as is the track efficiency which for this experiment was calculated using the kinematics of the $^2\mathrm{H}(\gamma,p)n$ reaction. Since the energy of the emitted proton is well above threshold at all measurable angles (17° to 163°), the track efficiency is close to 100% over the entire angular range of the detector.

The angular resolution function σ, describing the uncertainty in proton track angle, was determined from the uncertainties in the z determinations of the wire chamber hits and scintillator hits. This function varied from a minimum of $\sigma = 0.5°$ at $\theta_{\mathrm{lab}} = 20°$ and 160°, to a maximum of $\sigma = 5.5°$ at $\theta_{\mathrm{lab}} = 90°$. The validity of this procedure was verified previously by measurement of the $^1\mathrm{H}(p,p)^1\mathrm{H}$ cross section, using a 45 MeV proton beam [25].

The raw data contained mostly electron tracks, accounting for more than 97% of the total events collected. In order to remove these, it was necessary to apply data cuts based on the differential energy loss dE/dx of particles passing through the wire chamber (wire dE/dx) and scintillators (plastic dE/dx). In addition, a vertex radius cut of 8 cm was applied, as well as a χ^2 cut on the track fitted to each set of wire and plastic hits. These cuts are summarized in Table I, showing that about 99% of the proton tracks are preserved after the cuts are made. As previously shown [25], almost all electrons and cosmic-ray tracks are rejected from the data by these cuts.

Prior to making these cuts, a loose tape reduction cut was made on the data, according to the formula

$$(0.25E + \Delta E) > 5 \text{ MeVee} ,$$

where E and ΔE are the pulse heights in the thick and thin plastic scintillators, respectively. This cut was effective in eliminating most of the electron and cosmic-ray tracks prior to track fitting, allowing a significant saving in computer time during analysis. The number of proton tracks lost by this data-reduction cut was estimated in the calculation of the track efficiency, using the Monte Carlo code GEANT [27] (version 3.1305). The number lost is less than 2% for angles forward of $\theta_{\mathrm{c.m.}} = 140°$, 4% at 150° and increases to 8% at 160°.

TABLE I. Percentages of tracks excluded by data cuts.

Data cut	Proton tracks excluded (%)
Wire $dE/dx > 1.2$ keVee/cm	(0.03 $\pm$ 0.02)
Plastic $dE/dx > 8$ MeVee/cm	(0.20 $\pm$ 0.05)
8-cm vertex radius	(0.5 $\pm$ 0.2)
χ^2 cut on tracking	(0.18 $\pm$ 0.05)
Tagging coincidence cut	(0.0 $\pm$ 0.2)
Total excluded	(0.9 $\pm$ 0.3)

Histograms of the data at different stages of analysis are given in Figs. 2 and 3. Figure 2 shows the time-of-flight spectrum and Fig. 3 the angular distributions. In Figs. 2(a) and 3(a) electrons dominate the spectrum and protons are not at all discernible. After the loose tape reduction cut, the electrons and protons already show up as separate peaks in the time-of-flight histogram in Fig. 2(b). The electron peak is at 3.5 ns, while the proton peak is at 6.3 ns. Protons, which form a broad distribution centered around 75° in the angular distribution histogram in Fig. 3(b), are separated from electrons, which are forward peaked. After the more stringent cuts, Figs. 2(c) and 3(c) indicate almost complete removal of the electrons. The flat background in the time-of-flight histogram in Fig. 2(c) is due to random protons and a 1% contribution due to random electrons. The random protons result from photoproduction by the untagged part of the bremsstrahlung spectrum. They form a flat background because they are uncorrelated in time to the focal-plane electrons. These random proton tracks were subtracted from the data by selecting a region in the timing histograms where protons were kinematically forbidden and subtracting a proportionate amount from the region where the correlated protons were kinematically allowed.

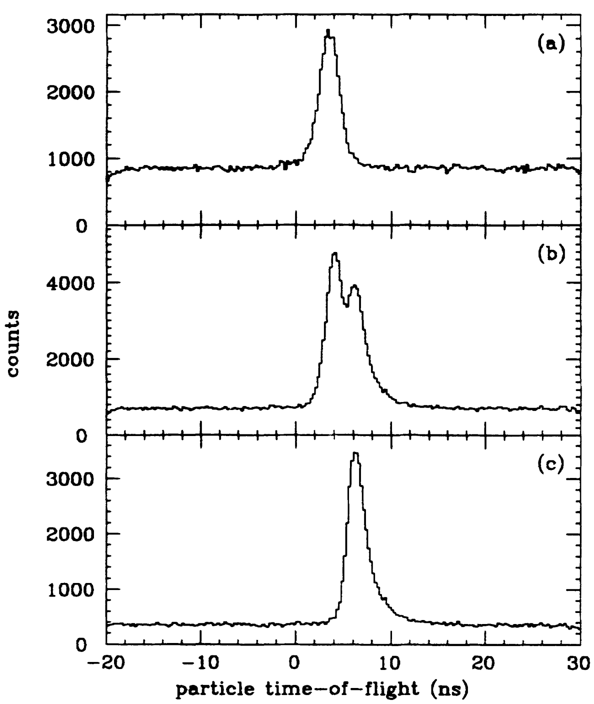

FIG. 2. Histograms of particle times of flight, for the full photon range, taken from event samples at various stages of analysis: (a) events that made a track using 1.1% of the data, (b) events that made a track following tape reduction cuts of $(0.25\,E + \Delta E) > 5$ MeVee using 36% of the data, and (c) events, following tape-reduction cuts, that made a track with wire $dE/dx > 1.2$ keVee/cm and plastic $dE/dx > 8$ MeVee/cm using 36% of the data. The peak at 3.5 ns corresponds to electrons, while the peak at 6.3 ns corresponds to protons.

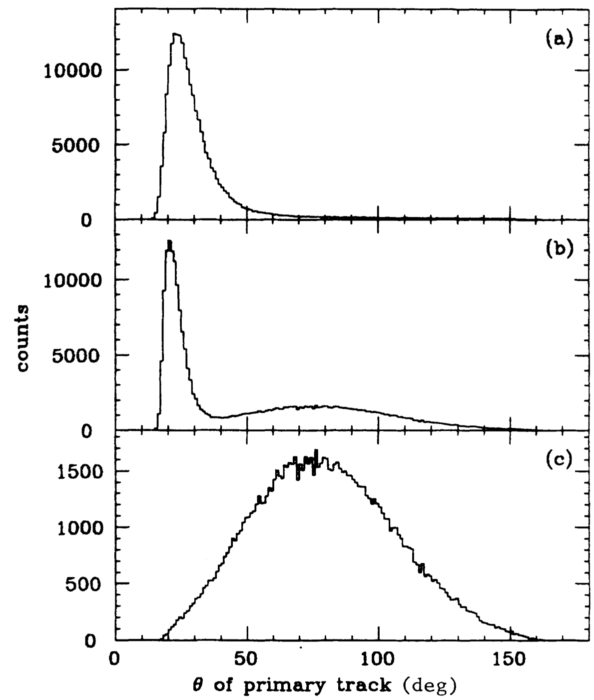

FIG. 3. Histograms of the laboratory polar angle θ, for the full photon range, for event samples at various stages of analysis: (a) events that made a track using 1.1% of the data, (b) events that made a track following tape reduction cuts of $(0.25E + \Delta E) > 5$ MeVee using 36% of the data, and (c) events, following tape-reduction cuts, that made a track with wire $dE/dx > 1.2$ keVee/cm and plastic $dE/dx > 8$ MeVee/cm using 36% of the data. The peak at about 21° corresponds to electrons, while the broad distribution centered at about 75° corresponds to protons.

The peak in Fig. 3 at about 21° corresponds to tracks with small dE/dx values, indicating a minimum ionizing particle. These have been identified as electrons from pair production upstream of the chamber. The broad distribution centered at about 75° corresponds to protons. During the experiment, efforts were made to keep the ratio of electron tracks to proton tracks as low as possible, using sweeping magnets upstream of the detector, along with secondary collimation to block off-axis particles in the beam. However, the bulk of the background elimination had to be done during analysis, after tracks had been fitted. As can be seen from Fig. 3, the electrons can be effectively discriminated against by the wire and plastic dE/dx cuts.

V. SYSTEMATIC UNCERTAINTIES

In order to obtain the $^2\mathrm{H}(\gamma,p)n$ cross section, it was necessary to subtract the contribution due to the (1.7 $\pm$ 0.4)% impurity by volume of air and (0.13 $\pm$ 0.01)% of ^{4}He. The spectrum to subtract, corresponding to the air impurity, was measured by collecting events with N_2 gas in the target chamber. The spectrum corresponding to ^{4}He was determined in the same way. The counts

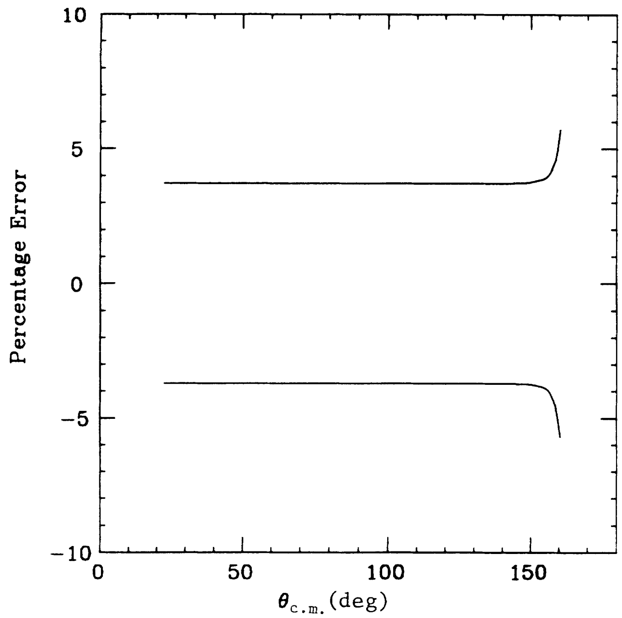

FIG. 4. The systematic uncertainty on the measured differential cross section as a function of angle.

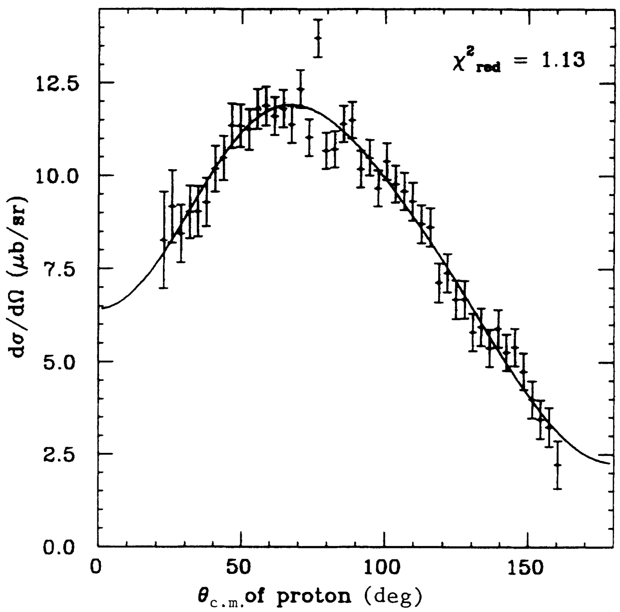

FIG. 5. The measured differential cross section for the $^2H(\gamma,p)n$ reaction, at an average energy of 67 MeV. The error bars shown are statistical only. The solid line is a Legendre polynomial fit to fourth order.

subtracted in making these corrections amounted to 13% of the raw spectra. The systematic uncertainty, due to the impurity corrections, amounted to 3.2% of the cross-section scale.

The systematic uncertainty due to the data cuts described in Table I amounts to ±0.3%. The uncertainty in measuring the tagging efficiency is ±1%. Similarly, the uncertainty in calculating the geometric acceptance is ±1%. The calculation of the track efficiency, using the code GEANT [27], contributed a systematic uncertainty to the final cross section that ranges from 0.2% at angles forward of $\theta_{c.m.} = 100°$, increasing to 0.5% at 130°, 1% at 150°, and 4.5% at 160°. This uncertainty arises mostly from a 0.6 MeVee uncertainty in the proton detection threshold of approximately 5 MeVee. The combined systematic uncertainty from all the above causes is plotted in Fig. 4, showing that the largest uncertainty is at the most backward angles.

VI. RESULTS

The measured cross section for the $^2H(\gamma,p)n$ reaction, at an average laboratory energy of 67 MeV, is shown in Fig. 5, and the cross-section values are listed in Table II. This spectrum was produced by summing all 32 focal plane channels, covering the photon energy range of 63 to 71 MeV, after the contributions from the N_2 and He impurities and the uncorrelated proton background were subtracted. Similarly, the $^2H(\gamma,p)n$ cross section was estimated at energies of 64.0, 65.8, 67.8, and 70.0 MeV, by summing the focal plane channels in groups of eight. Superimposed on the cross section in Fig. 5 is a Legendre polynomial fit to fourth order. In making this fit, the differential cross section in the c.m. frame was represented by the usual Legendre polynomial expansion:

TABLE II. The $^2H(\gamma,p)n$ differential cross section at laboratory energy $E_\gamma = 66.9$ MeV, as measured in this reported experiment for the energy range 63–71 MeV. The errors are given as cross section ± statistical error ± systematic error. The systematic error is 3.7%.

$\theta_{c.m.}$ (deg)	c.m. cross section (μb/sr)	$\theta_{c.m.}$ (deg)	c.m. cross section (μb/sr)
22.5	8.3 ± 1.3 ± 0.3	94.5	10.5 ± 0.5 ± 0.4
25.5	9.2 ± 1.0 ± 0.3	97.5	9.7 ± 0.5 ± 0.4
28.5	8.4 ± 0.8 ± 0.3	100.5	10.4 ± 0.5 ± 0.4
31.5	9.0 ± 0.7 ± 0.3	103.5	9.8 ± 0.5 ± 0.4
34.5	9.0 ± 0.7 ± 0.3	106.5	9.6 ± 0.5 ± 0.4
37.5	9.3 ± 0.7 ± 0.3	109.5	9.3 ± 0.5 ± 0.3
40.5	10.2 ± 0.6 ± 0.4	112.5	8.7 ± 0.5 ± 0.3
43.5	10.5 ± 0.6 ± 0.4	115.5	8.6 ± 0.5 ± 0.3
46.5	11.4 ± 0.6 ± 0.4	118.5	7.1 ± 0.5 ± 0.3
49.5	11.3 ± 0.6 ± 0.4	121.5	7.4 ± 0.5 ± 0.3
52.5	11.2 ± 0.6 ± 0.4	124.5	6.7 ± 0.5 ± 0.3
55.5	11.8 ± 0.5 ± 0.4	127.5	6.7 ± 0.5 ± 0.3
58.5	11.9 ± 0.5 ± 0.4	130.5	5.8 ± 0.5 ± 0.2
61.5	11.6 ± 0.5 ± 0.4	133.5	5.9 ± 0.5 ± 0.2
64.5	11.8 ± 0.5 ± 0.4	136.5	5.4 ± 0.5 ± 0.2
67.5	11.4 ± 0.5 ± 0.4	139.5	5.9 ± 0.5 ± 0.2
70.5	12.3 ± 0.5 ± 0.5	142.5	5.3 ± 0.5 ± 0.2
73.5	11.0 ± 0.5 ± 0.4	145.5	5.4 ± 0.5 ± 0.2
76.5	13.7 ± 0.5 ± 0.5	148.5	4.7 ± 0.5 ± 0.2
79.5	10.7 ± 0.5 ± 0.4	151.5	4.0 ± 0.5 ± 0.2
82.5	10.7 ± 0.5 ± 0.4	154.5	3.4 ± 0.5 ± 0.1
85.5	11.4 ± 0.5 ± 0.4	157.5	3.2 ± 0.5 ± 0.1
88.5	11.5 ± 0.5 ± 0.4	160.5	2.2 ± 0.6 ± 0.1
91.5	10.2 ± 0.5 ± 0.4		

TABLE III. Summary of the final cross-section parameters obtained by fitting a Legendre series of fourth order to the data. The statistical errors are listed along with the parameters. The systematic error is 3.7%. The quality of the fits is indicated by the χ^2 per degree of freedom listed in the right-hand column. The coefficients are in units of μb/sr.

	Fit coefficients with statistical errors					
Photon energy (MeV)	A_0	A_1	A_2	A_3	A_4	$\chi^2/N_{\mathrm{d.o.f.}}$
63–71	9.05±0.08	3.14±0.15	-4.08±0.23	-1.07±0.26	-0.63 ±0.30	47.4/42
64.0	9.73±0.14	2.88±0.25	-4.9±0.4	-0.7±0.5	-0.1±0.5	40.7/42
65.8	9.37±0.14	2.89±0.25	-4.5±0.4	-1.3±0.5	-1.1±0.5	51.4/42
67.8	8.95±0.10	3.12±0.25	-4.1±0.4	-1.1±0.4	-0.5±0.5	50.1/42
70.0	8.45±0.13	3.54±0.24	-3.0±0.4	-1.2±0.4	-0.6±0.5	30.5/42

$$\frac{d\sigma}{d\Omega} = \sum_{l=0}^{4} A_l(E_\gamma)P_l(\cos\theta) \ , \qquad (1)$$

where θ is the c.m. angle between the incoming photon and outgoing proton. The coefficients of the fit shown in Fig. 5, and fits made to the cross-section estimates at 64.0, 65.8, 67.8, and 70.0 MeV can be found in Table III.

To estimate the effect of the angular dependence of the systematic error, shown in Fig. 4, on the uncertainty in the Legendre coefficients, the coefficients were determined by a fit that included an angle-dependent error. The resulting coefficients and uncertainties were substantially the same as when only statistical errors were considered. This is due to the size of the statistical error in the cross section that, at large angles, dominates the uncertainty introduced by changes in the systematic error. For example, at 160.5° the cross section has a statistical error of 27% whereas the systematic error varies from 3.7% at 148.5° to 5.7% at 160.5°. Therefore the angle dependence of the systematic error is not significant and has been neglected in the analysis. The systematic error of 3.7% is regarded as a normalization error and must be considered as part of the total uncertainty in the Legendre coefficients.

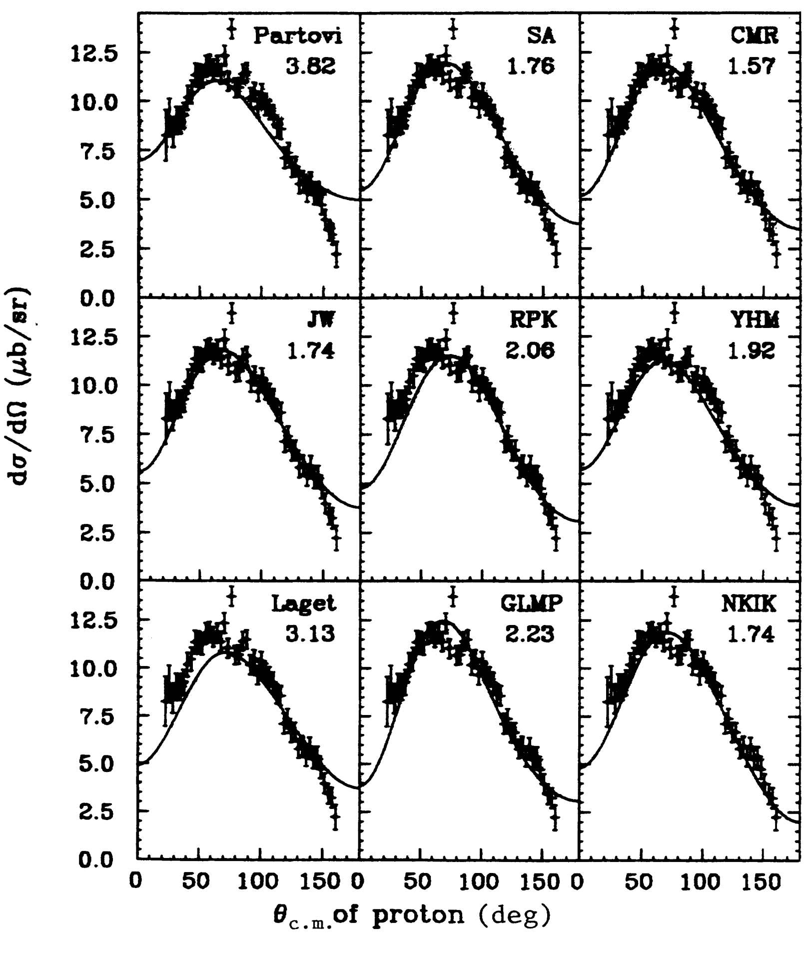

FIG. 6. The measured differential cross section for the ^{2}H$(\gamma,p)n$ reaction, at an average energy of 67 MeV, compared to theoretical calculations by Partovi, SA, CMR, JW, RPK, YHM, Laget, and GLMP, all at 67 MeV, and NKIK, at 68 MeV. The reduced χ^2 values are shown for each case.

TABLE IV. Summary of the Legendre coefficients obtained by fitting a Legendre series of fourth order to each of the nine theoretical calculations discussed. The quality of the agreement with the data is indicated by the χ^2 per degree of freedom listed in the right-hand column. The coefficients are in units of μb/sr. The measured coefficients are given with statistical and systematic errors added in quadrature.

Calculation	A_0	A_1	A_2	A_3	A_4	$\chi^2/N_{d.o.f.}$
CMR(IA)	8.60	2.59	-2.39	-1.66	-0.38	3.65
CMR(IA+MEC)	9.40	2.64	-3.17	-1.73	-0.41	2.77
CMR(full)	8.80	2.67	-4.00	-1.85	-0.45	1.57
JW	8.97	2.53	-3.90	-1.65	-0.41	1.74
NKIK	8.68	2.86	-4.86	-1.46	-0.43	1.74
SA	9.12	2.51	-4.08	-1.63	-0.41	1.76
YHM	8.60	2.50	-3.44	-1.60	-0.37	1.92
RPK	8.61	2.30	-4.57	-1.47	-0.13	2.06
GLMP	8.82	2.96	-4.80	-2.59	-0.56	2.23
Laget	8.47	1.80	-3.76	-1.22	-0.39	3.13
Partovi	8.71	2.48	-2.39	-1.50	-0.34	3.62
Measured	9.05±0.34	3.14±0.19	-4.08±0.28	-1.07±0.26	-0.63±0.30	

The present measurement of the ^{2}H$(\gamma,p)n$ cross section can be compared directly with several theoretical calculations of the cross section. Figure 6 shows the ^{2}H$(\gamma,p)n$ cross section at 67 MeV, as calculated by Partovi, SA, CMR, JW, RPK, YHM, Laget, and GLMP superimposed on the data of the present measurement. The calculation by NKIK for the ^{2}H$(\gamma,p)n$ cross section at 68 MeV is also shown.

The reduced χ^2 values were calculated using the definition of χ^2 given by Arndt and MacGregor [28]:

$$\chi^2 = \sum_{i=1} \left(\frac{N\sigma_i^{\rm th} - \sigma_i^{\rm exp}}{\epsilon_i}\right)^2 + \left(\frac{N-1}{\epsilon_N}\right)^2 , \qquad (2)$$

where $\sigma_i^{\rm th}$ is the calculated cross section at each data angle, $\sigma_i^{\rm exp}$ is the experimental cross section at each data angle, ϵ_i is the error on each experimental data point, ϵ_N is the normalization uncertainty, and N is the normalization constant which minimizes χ^2 and is given by

$$N = \frac{1 + \epsilon_N^2 \sum_{i=1} \sigma_i^{\rm th}\sigma_i^{\rm exp}/\epsilon_i^2}{1 + \epsilon_N^2 \sum_{i=1} \left(\sigma_i^{\rm th}/\epsilon_i\right)^2} . \qquad (3)$$

The χ^2 value was then divided by 42, the number of degrees of freedom, to give the reduced χ^2. The values obtained in this way are shown for each calculation in Fig. 6.

The Legendre coefficients corresponding to each of the calculations are shown in Table IV. For the calculations by Partovi, SA, CMR, and GLMP the coefficients were provided by the theorists at regularly spaced photon energies, and so interpolations were made in order to obtain the coefficients at 67 MeV. For the calculation by RPK the coefficients were provided at 67 MeV. The others, JW, YHM, Laget, and NKIK, provided differential cross sections, to which least-squares Legendre polynomial fits up to fourth order have been made. In the case of YHM and NKIK the cross sections were given at the experimental photon energy, but for JW and Laget interpolations were required.

For the calculation by CMR the coefficients were provided for three different cases: the full calculation (IA+MEC+RC), a semicomplete calculation (IA+MEC), and the basic IA calculation. These three versions of the CMR calculation are plotted in Fig. 7, along with the data. Table IV contains the reduced χ^2 values for each of the three cases.

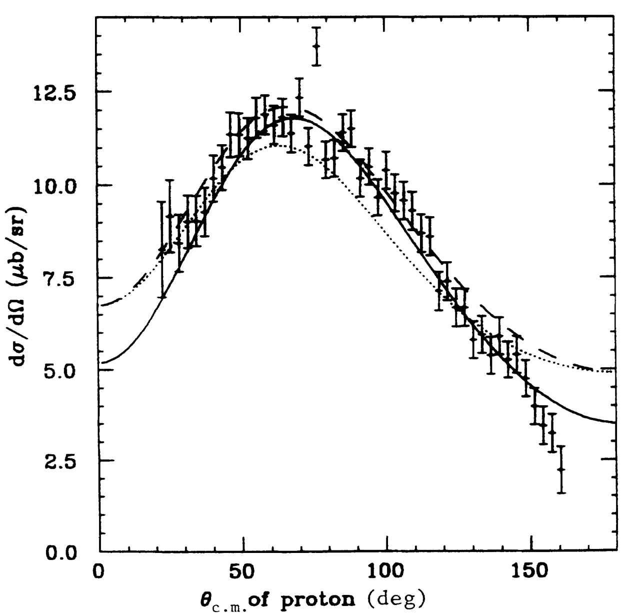

FIG. 7. Comparison of the present data with the CMR full calculation (IA+MEC+RC) (solid line), semicomplete CMR calculation (IA+MEC) (dashed line), and basic IA calculation by CMR (dotted line).

VII. DISCUSSION

It can be seen in Fig. 6 that the best agreement with the data is obtained with the calculations SA, CMR, and JW, which are all very similar. This is to be expected, since the three calculations only differ significantly in their calculation of the IC contribution [1], which has only a small effect at the energies of the present measurement. The agreement of the NKIK calculation with the data is as good as for the above three calculations. NKIK give smaller cross section values at forward and backward angles than the three calculations SA, CMR, and JW. This improves the agreement with the data at the backward angles, and offsets the poorer agreement at forward angles in the calculation of χ^2.

Somewhat poorer agreement is obtained for the YHM and RPK calculations. The disagreement of the YHM calculation with experimental data becomes much larger at higher photon energies, as shown by Wallace *et al.* [29], in a comparison to their data at 140 MeV. In the present comparison YHM gives cross-section values that are smaller than the data over most of the angular range, except for angles ($\theta_{\rm c.m.}$) greater than 120°. RPK gives lower values at forward angles, but fair agreement at backward angles. Slightly worse is the agreement with the low-energy-theorem calculation GLMP that deviates most from the data at forward angles. GLMP gives the lowest 0° cross section of the nine calculations. Still poorer agreement is obtained from the Laget calculation, which lies about 15% lower than the data, for angles ($\theta_{\rm c.m.}$) forward of 70°. As might be expected, the nonrelativistic calculation by Partovi gives the highest χ^2 value when compared to the data. This demonstrates that without the MEC beyond the Siegert operators, IC and RC, the discrepancy between theory and data is noticeably worse.

In Fig. 7 and Table IV it can be seen that for the three versions of the CMR calculation, the best agreement is obtained for the full calculation. The IA curve is almost identical to that calculated by Partovi, with high values of the cross section at 0° and 180°, and lower cross section values in between, compared to other calculations.

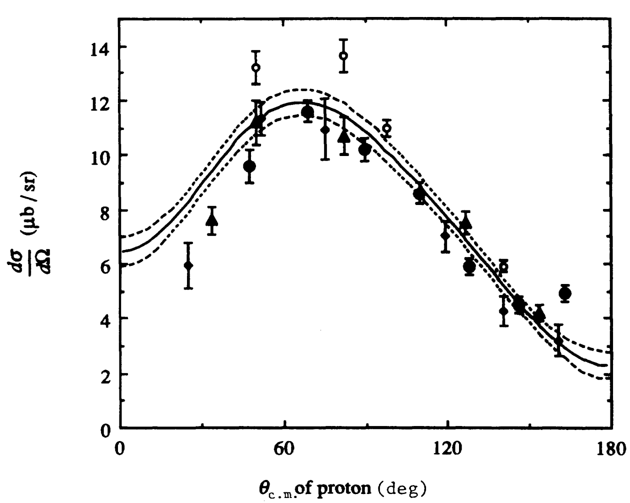

FIG. 8. Comparison of the present data, as represented by the solid line from Fig. 5, with the data of Galey [4], open circle (65 MeV data); Whalin *et al.* [2], solid triangle (65 MeV data); Krause *et al.* [8, 9], solid circle (68 MeV data); and Aleksandrov *et al.* [3], solid diamond (70 MeV data). The dashed lines above and below the solid line represent the error envelope of the present measurement, and includes both statistical and systematic errors to one standard deviation.

The close similarity to the Partovi curve indicates that at this photon energy the use of the Hamada-Johnston potential by Partovi does not adversely affect the cross section calculation. The IA+MEC curve of Fig. 7 shows that the additional MEC contributions increase the cross section at angles away from 0° and 180°, to about the size indicated by the data. The addition of RC to complete the calculation reduces the cross section at 0° and 180°, while making only a small decrease in cross section at the midrange angles. As seen in Table IV, there is a clear improvement in the reduced χ^2, when the additional MEC and RC contributions are included in the calculation. It is evident from the Legendre coefficients in Table IV that the inclusion of MEC and RC into the calculation mostly affects the A_2 coefficient.

While the present measurement is able to distinguish which of the calculations best describe the ${}^2{\rm H}(\gamma,p)n$ cross section at these energies, it is also evident that measurements at 0° and 180° would be invaluable for differentiating between the different theoretical curves, since they differ most at these extremes.

A comparison of the present measurement with earlier work is shown in Fig. 8. Good agreement is obtained with the data of Krause *et al.* [8], except for the point at 164°, and with the data of Aleksandrov *et al.* [3] and Whalin *et al.* [2] except for the forwardmost angles. The results of Galey [4] are systematically higher than the present work.

A comparison of measured A_l coefficients, for the Legendre expansion of the angular distribution of Eq. (1), is given in Fig. 9. By comparing the ratio A_l/A_0, differences in normalization between experiments are removed. The coefficients and errors presented in the figure were computed using the procedure described by Bevington [30]. Only statistical errors are used in the calculation. The comparison includes only those experiments that reported cross sections for a sufficient range of angles to determine the A_l coefficients. The A_4/A_0 coefficient could not be calculated for Galey's data since only four angles were reported at each energy. As shown in the figure, the data reported by the different groups are in fair agreement with each other and with the calculation of SA; however, the A_1/A_0 coefficient of the present work at 70 MeV and the data of Cameron *et al.* for the inverse reaction at 92 MeV are substantially greater than the prediction of SA. The other data for the A_1/A_0 coefficient tend to lie above the SA prediction, but the differences are hidden by large errors. A similar systematic deviation has been observed for data between 10 and 40 MeV [31].

The present measurement of the Legendre coefficients is compared to different theories in Fig. 10. At 64 MeV the data for the A_1/A_0 coefficient agrees with SA, JW, CMR, and Partovi, but it disagrees with Laget, which is consistently less than the other calculations. As energy increases, the measured coefficient increases more rapidly than the calculations. The A_2/A_0 coefficient agrees with the calculations shown except for Partovi. The Partovi value for A_2 is the same as calculated by CMR when MEC and RC are omitted. The A_3/A_0 coefficient tends to agree with the calculations shown except for CMR.

The A_4/A_0 coefficient agrees with calculation, but the errors are too large for a useful comparison between calculations.

The Legendre coefficients, derived from a fit to the data, can be used in Eq. (1) to calculate the cross sections at 0° and 180°. These cross sections are a sensitive probe of spin-dependent transition operators, the deuteron D state, noncentral forces, and subnuclear degrees of freedom [1, 32]. The Legendre coefficients derived from the data set, which extends from 63 to 71 MeV, predict a 0° cross section of 6.41±0.54 μb/sr and a 180° cross section of 2.27±0.50 μb/sr. At 67 MeV, SA calculate a 0° cross section of 5.51 μb/sr and at 180° a cross section of 3.75 μb/sr. The 0° cross section derived from the present measurement is somewhat greater than the 77-MeV measurement of Hughes of 4.3±0.2 μb/sr [33]. At 77 MeV, SA calculate a 0° cross section of 5.20 μb/sr.

The total cross section can be compared to the measurements of Bernabei *et al.*, who measured the cross section using a monochromatic photon beam and a very large angular acceptance detector for the proton [34]. Their cross sections at 47.5, 57.5, and 74.0 MeV are given, with the present measurement and a comparison to the calculation of SA, in Fig. 11. The measurements are consistent with each other and with the calculation. The present measurement of the total cross section is

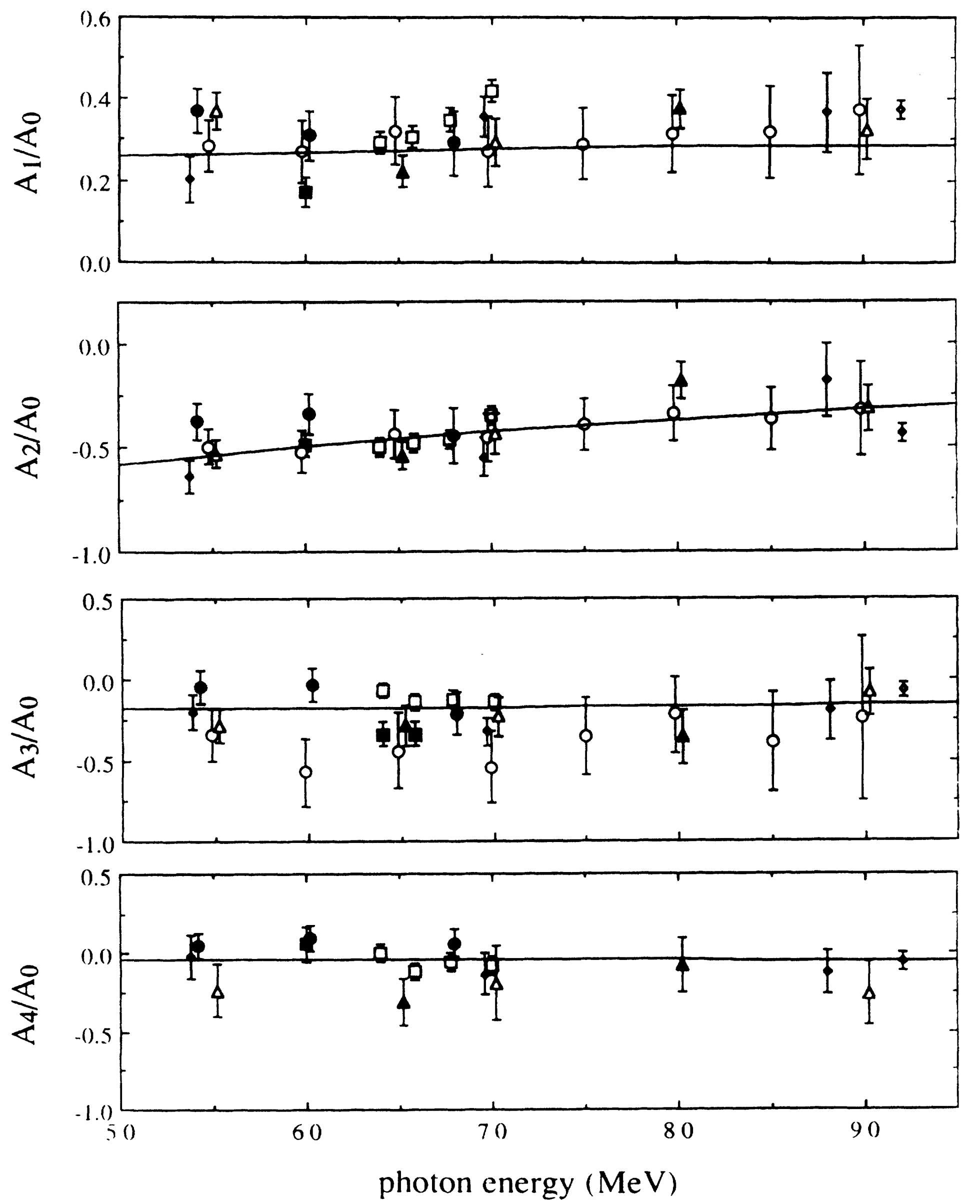

FIG. 9. Legendre coefficients compared to SA (solid line). The notation is the same as in Fig. 8, with the addition of Cameron *et al.* [10], open diamond at 92 MeV; De Pascale *et al.* [7], solid square; Shin *et al.* [5], open triangle; and the present data, open square.

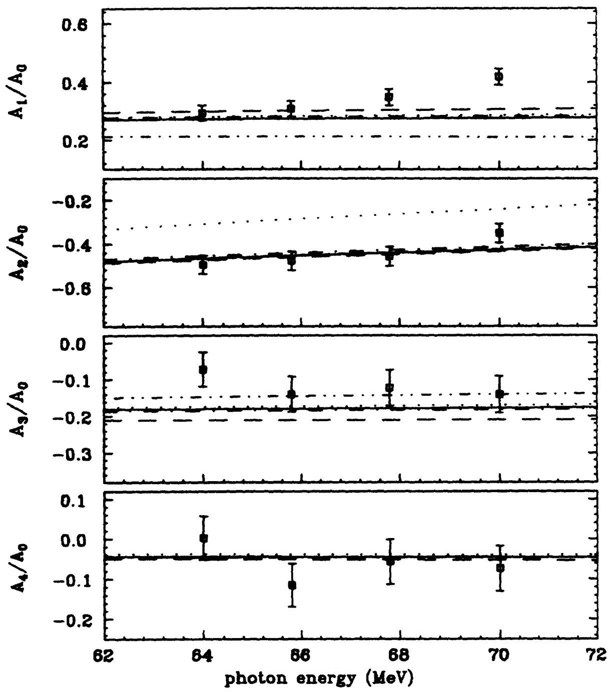

FIG. 10. Comparison of the present measurement of the Legendre coefficients with the calculations by SA (solid line), JW (dot-dashed line), CMR (dashed line), Partovi (dotted line), and Laget (dot-dot-dashed line).

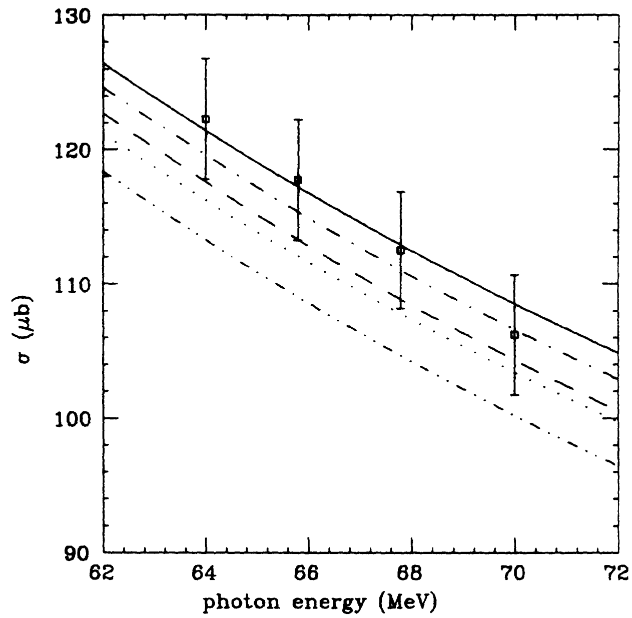

FIG. 12. Comparison of the present measurement of the total cross section with the calculations by SA (solid line), JW (dot-dashed line), CMR (dashed line), Partovi (dotted line), and Laget (dot-dot-dashed line). The errors on the data include statistical and systematic errors added in quadrature.

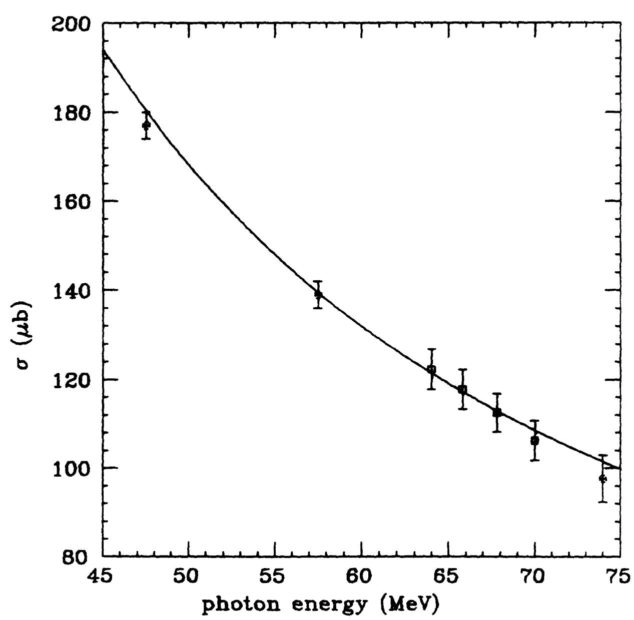

FIG. 11. Comparison of the total cross-section measurements of Bernabei *et al.* [34] (cross) and the present work (square) with statistical and systematic errors added in quadrature. The solid line is the calculation of SA.

compared to different calculations in Fig. 12. The best agreement is found with the calculation of SA.

VIII. SUMMARY AND CONCLUSIONS

The differential cross section for the $^2\mathrm{H}(\gamma,p)n$ reaction has been measured for tagged photon energies from 63 to 71 MeV, over the angular range from 22.5° to 160.5°. The average statistical error on each data point, representing an angular bin of 3°, is about 5% in the angular region near the cross section peak. The systematic error is less than 4%, for all but the highest few angles measured.

Comparison of the data has been made with nine theoretical calculations of the $^2\mathrm{H}(\gamma,p)n$ cross section. The differences in the calculated curves can be quantitatively assessed by the χ^2 agreements with the data. The data are of sufficient quality to distinguish which of the calculations gives a better description of the cross-section angular distribution.

ACKNOWLEDGMENTS

This work has been supported by the National Science Foundation under Grants No. NSF-PHY85-20738, No. NSF-PHY86-10493, No. NSF-PHY89-21146, and No. NSF-PHY91-12528. We acknowledge the interest and encouragement of Professor H. Arenhövel, Professor R. A. Arndt and Dr. J. L. Friar.

[1] H. Arenhövel and M. Sanzone, Few Body Syst. Suppl. **3** (1991).
[2] E. A. Whalin, B. D. Schriever, and A. O. Hanson, Phys. Rev. **101**, 377 (1956).
[3] Iu. A. Aleksandrov, N. B. Delone, L. I. Slovokhotov, G. A. Sokol, and L. N. Shtarkov, Zh. Eksp. Teor. Fiz. **33**, 614 (1957) [Sov. Phys JETP **6**, 472 (1958)].
[4] J. A. Galey, Phys Rev. **117**, 763 (1960).
[5] Y. M. Shin, R. A. Rawlins, W. Buss, and A. O. Evwaraye, Nucl. Phys. **A154**, 482 (1970).
[6] M. P. De Pascale, G. Giordano, G. Matone, P. Picozza, L. Azario, R. Caloi, L. Casano, L. Ingrosso, M. Mattioli, E. Poldi, D. Prosperi, and C. Schaerf, Phys. Lett. **119B**, 30 (1982).
[7] M. P. De Pascale, G. Giordano, G. Matone, D. Babusci, R. Bernabei, O. M. Bilaniuk, L. Casano, S. d'Angelo, M. Mattioli, P. Picozza, D. Prosperi, C. Schaerf, S. Frullani, and B. Girolami, Phys. Rev. C **32**, 1830 (1985).
[8] K. H. Krause, J. Sobolewski, J. Ahrens, J. M. Henneberg, and B. Ziegler, *Physics with MAMI A: 1983-1987*, Institut für Kernphysik, Johannes Gutenberg-Universitat, Mainz, 1988 (unpublished).
[9] K. H. Krause, J. Sobolewski, J. Ahrens, J. M. Henneberg, and B. Ziegler, in *Proceedings of the Workshop on Nuclear Physics with Real Photons below Pion Threshold, Gent, 1989*, edited by D. Ryckbosch (Laboratorium voor Kernfysica, Gent University, Gent, Belgium); private communication.
[10] J. M. Cameron, C. A. Davis, H. Fielding, P. Kitching, J. Pasos, J. Soukup, J. Uegaki, J. Wesick, H. S. Wilson, R. Abegg, D. A. Hutcheon, C. A. Miller, A. W. Stetz, and I. J. Van Heerden, Nucl. Phys. **A458**, 637 (1986).
[11] H. O. Meyer, J. R. Hall, M. Hugi, H. J. Karwowski, R. E. Pollock, and P. Schwandt, Phys. Rev. C **31**, 309 (1985).
[12] F. Partovi, Ann. Phys. **27**, 79 (1964).
[13] T. Hamada and I. D. Johnston, Nucl. Phys. **34**, 382 (1962).
[14] K.-M. Schmitt and H. Arenhövel, Few Body Syst. **7**, 95 (1989); private communication.
[15] A. Cambi, B. Mosconi, and P. Ricci, J. Phys. G **10**, L11 (1984); private communication.
[16] W. Jaus and W. S. Woolcock, Nucl. Phys. **A473**, 667 (1987); private communication.
[17] M. L. Rustgi, L. N. Pandey and A. Kassaee, Phys. Rev. C **33**, 1823 (1986); private communication.
[18] S. Ying, E. M. Henley, and G.A. Miller, Phys. Rev. C **38**, 1584 (1988); private communication.
[19] K.-M. Schmitt, P. Wilhelm, H. Arenhövel, A. Cambi, B. Mosconi, and P. Ricci, Phys. Rev. C **41**, 841 (1990).
[20] J. M. Laget, Can. J. Phys. **62**, 1046 (1984); Phys. Lett. B **199**, 493 (1987); private communication.
[21] J. Govaerts, J. L. Lucio, A. Martinez, and J. Pestieau, Nucl. Phys. **A368**, 409 (1981); J. L. Lucio, A. Martinez, and J. Pestieau, Nuovo Cimento **89**, 292 (1985).
[22] S. I. Nagornyi, Yu. A. Kasatkin, E. V. Inopin, and I. K. Kirichenko, Yad. Fiz. **44**, 1171 (1986) [Sov. J. Nucl. Phys. **44**, 760 (1986)]; private communication.
[23] P. Axel, L. S. Cardman. R. A. Daniel, A. O. Hanson, R. A. Hoffswell, R. M. Laszewski, W. C. Sellyey, N. Towne, and A. M. Vetter, IEEE Trans. Nucl. Sci. **NS-30**, 1112 (1983).
[24] Jonathan E. Knott, Ph.D. thesis, University of Illinois, 1988.
[25] P. D. Harty, R. T. Jones, J. E. Knott, P. T. Debevec, and D. A. Jenkins, Nucl. Instrum. Methods **A297**, 415 (1990).
[26] R. T. Jones, D. A. Jenkins, P. T. Debevec, P. D. Harty, and J. E. Knott, Phys. Rev. C **43**, 2052 (1991).
[27] R. Brun, F. Bruyant, M. Maire, A. C. McPherson, and P. Canarini, CERN Data Handling Division, Geneva, DD/EE/84-1, 1987 (unpublished).
[28] R. A. Arndt and M. H. MacGregor, in *Methods in Computational Physics* (Academic, New York, 1966), Vol. 6, pp. 253–296.
[29] P. A. Wallace, J. R. M. Annand, I. Anthony, G. I. Crawford, S. N. Dancer, S. M. Doran, S. J. Hall, J. D. Kellie, J. C. McGeorge, I. J. D. McGregor, G. J. Miller, R. O. Owens, J. Vogt, B. Schoch, and D. Branford, Nucl. Phys. **A532**, 617 (1991).
[30] P. R. Bevington, *Data Reduction and Error Analysis for the Physical Sciences* (McGraw Hill, New York, 1969), Chap. 8.
[31] K.-M. Schmitt, P. Wilhelm, and H. Arenhövel, Few Body Syst. **10**, 105 (1991).
[32] J. L. Friar, B. F. Gibson, and G. L. Payne, Phys. Rev. C **30**, 441 (1984).
[33] R. J. Hughes, A. Zieger, H. Waffler, and B. Ziegler, Nucl. Phys. **A267**, 329 (1976).
[34] R. Bernabei, A. Incicchitti, M. Mattioli, P. Picozza, D. Prosperi, L. Casano, S. d'Angelo, M. P. De Pascale, C. Schaerf, G. Giordano, G. Matone, S. Frullani, and B. Girolami, Phys. Rev. Lett. **57**, 1542 (1986).